Finite element modeling of creep deformation in cellular metals

Scott M. Oppenheimer, David C. Dunand *

Department of Materials Science and Engineering, Northwestern University, Evanston, IL 60208, USA

Abstract

The creep of reticulated metallic foams is studied through the finite element method using three-dimensional, periodic unit cells with four different architectures characterized by struts which deform primarily by: (i) simple bending, (ii) compression, (iii) a combination of simple bending and compression and (iv) double bending (for Kelvin space-filling tetrakaidecahedra). The creep behavior of each of these models is examined with respect to temperature, stress and foam relative density. Calculated creep rates for both bending and compression models are below those predicted from simplified analytical models and bracket those of the combination model. The simple and double bending models predict nearly identical strain rates despite very different geometries, because in both cases the deflection rates of the fastest deforming struts are similar. Both analytical and numerical predictions are compared to published creep data for metallic foams.

1. Introduction

Metallic foams are well suited for use at elevated temperatures in structural (e.g. as load-bearing sandwiches in hot environments) and non-structural applications (e.g. as heat exchangers, filters, catalyst substrates and fuel cell interconnects) [1], because they show much better resistance to creep deformation and oxidation than polymeric foams and much better toughness, thermal conductivity and thermal shock resistance than ceramic foams. The limited number of studies that exist on the mechanical properties of metallic foam at high temperatures have focused mainly on aluminium and nickel foams [2–13]. In these studies, experimental results were compared to predictions from two analytical models for foam creep. The first model, originally developed by Gibson and Ashby [14], applies to open-cell, reticulated foams whose deformation is controlled by the creep bending of struts perpendicular to the applied stress, with struts parallel to the stress

assumed to remain rigid (Fig. 1a). Considering a cubic array of struts and using dimensional arguments, these authors derived the following relationship for the strain rate $\dot{\varepsilon}$ of the foam:

$$\dot{\varepsilon} = A \frac{0.6}{n+2} \left(\frac{1.7(2n+1)}{n} \right) \sigma^n \rho^{-(3n+1)/2} \exp\left(-\frac{Q}{RT} \right) \qquad (1)$$

where σ is the uniaxial stress applied to the foam, ρ is the foam relative density (ratio of foam and solid density) and the other variables are related to the power law creep equation for the solid material of which the foam consists:

$$\dot{\varepsilon}_s = A\sigma_s^n \exp\left(-\frac{Q}{RT} \right) \qquad (2)$$

In this equation, $\dot{\varepsilon}_s$ is the uniaxial strain rate, A is the creep constant, σ_s is the uniaxial stress, n is the stress exponent, Q is the creep activation energy, R is the gas constant and T is the temperature. This model was subsequently modified to take into account mechanisms other than power law creep (Eq. (2)), i.e. diffusional creep [2,8] and power law breakdown [9], as well as hollow strut geometries [2,8] and sandwich structures [1,15].

---

* Corresponding author. Tel.: +1 847 491 5370.
  E-mail address: dunand@northwestern.edu (D.C. Dunand).
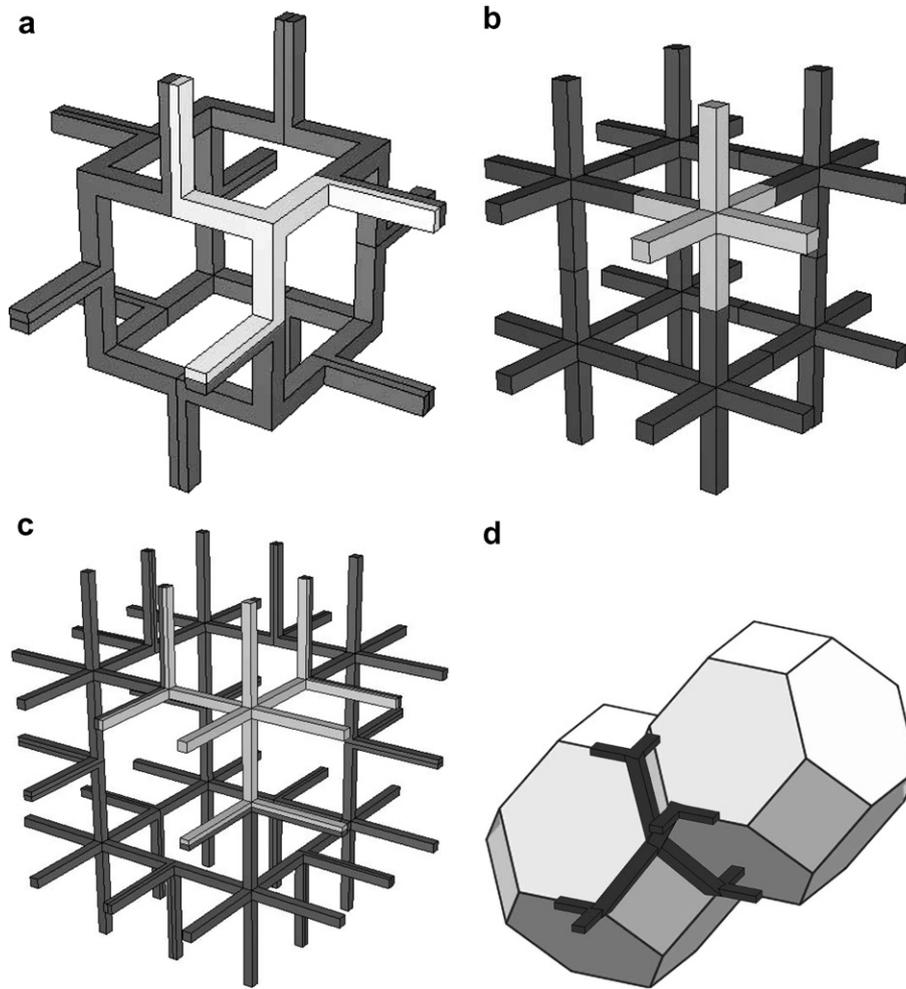
Fig. 1. Extended unit cell for four models studied: (a) B model, where struts deform by bending; (b) C model, where struts deform by compression; (c) BC model, combining aspects of both B and C models; and (d) S model, based on the tetrakaidecahedron geometry, where struts at 45° to applied stress (applied vertically for all models) deform by bending. Volume fractions are not uniform between models. Smaller unit cells used for FEM calculations (Fig. 2) are highlighted.

A second model, proposed by Hodge and Dunand [6], assumes a different reticulated architecture where struts perpendicular to the stress are prevented from bending, so that foam deformation is solely due to the uniaxial compressive deformation of struts parallel to the applied stress (Fig. 1b). The foam strain rate is then given by:

$$\dot{\varepsilon} = A \left(\frac{\rho}{3}\right)^{-n} \sigma^n \exp\left(-\frac{Q}{RT}\right) \qquad (3)$$

Finally, analytical models have also been developed for creep of honeycombs [16] and for creep buckling of foams [17].

Finite element modeling (FEM) can be used to provide a more realistic evaluation of the creep of the simple unit cells used in the above analytical models, e.g. by considering stress concentrations at nodes and by using periodic boundary conditions, taking into account the stress overlap between adjacent cells. FEM can also study unit cells with more complex architectures, permitting an evaluation of the sensitivity of the above equations to the geometry of

the unit cell. Some two-dimensional (2D) FEM studies exist for the creep of metallic foams [4,18,19] but very few three-dimensional (3D) FEM studies have been published to date, as summarized below.

Huang and Gibson [20] considered open-cell Voronoi foams with a relative density of 8%. Their unit cell consisted of a large number of struts (about 250) with periodic boundary conditions, each strut containing a small number (4) of linear beam elements. The model predicted that the foam shows the same stress- and temperature-dependence as the simplified analytical solution of Eq. (1), but the value of their constant A was higher by a factor 3; compared to experimental data on aluminium foams, the FEM analysis over-predicted creep rate by a factor 16. This study also compared the effect of uniform thinning of the struts and removal of individual struts and found that the latter damage led to much higher foam strain rates.

Hodge and Dunand [6] investigated the simple 3D cell geometry shown in Fig. 1b corresponding to the simplified analytical solution in Eq. (3); their model consisted of a

small number (6) of hollow or full struts meshed with a large number of elements with periodic boundary conditions. For relative densities of 5% and 5.5%, the FEM predictions were in good agreement with analytical results given by Eq. (3) and with creep rates measured on NiAl foams (within a factor 2).

Both analytical models – the model by Gibson and Ashby [14] where only transverse struts deform by bending (Fig. 1a, Eq. (1)) and the model by Hodge and Dunand [6] where only longitudinal struts deform by compression (Fig. 1b, Eq. (3)) – are by necessity very simplified. Since realistic foam architectures display struts that carry load in both bending and compression, more detailed models are needed. Here, using the FEM approach, we study a combination cell where some struts deform by bending and other by compression (Fig. 1c) and we also investigate a cell where struts are arranged in tetrakaidecahedral geometry and are subjected to simultaneous bending and compression (Fig. 1d). For these two more complex geometries (Fig. 1c–d) and for the two original simpler geometries (Fig. 1a–b), we carry out a parametric study where the foam creep rate is calculated as a function of strain, while varying foam relative density, stress and temperature. We also compare our results with experimental creep data previously published on cellular aluminium and nickel alloys.

2. Computational procedures

The four models are depicted in Fig. 2a–d for a constant relative density of 2.6%; by use of symmetry conditions; a smaller number of struts are shown than in the extended cell representation depicted in Fig. 1a–d. The first two models correspond to 3D versions of the original 2D models for which approximate close-form solutions exist (Eqs. (1) and (3)). The first model (Fig. 2a) deforms mostly by strut bending and is thus referred to as the B model. The second model (Fig. 2b) is controlled by strut compression and is thus labeled as the C model. The third model (Fig. 2c) is a combination of the above two models and contains struts that deform by bending (as in the B model) and by compression (as in the C model) and it is thus labeled as the BC model. The fourth model (Fig. 2d) is based on the tetrakaidecahedral geometry, which has often been used in models studying deformation at room temperature [21,22]. This model represents a Kelvin cell [22], displaying a periodic, space-filling arrangement of struts, some of which are perpendicular to the applied stress (like the other three models) and others that are at a 45° angle with the applied stress (unlike the other three models), providing a structure that may be closer to actual stochastic foams. As described later in more detail, struts tend to
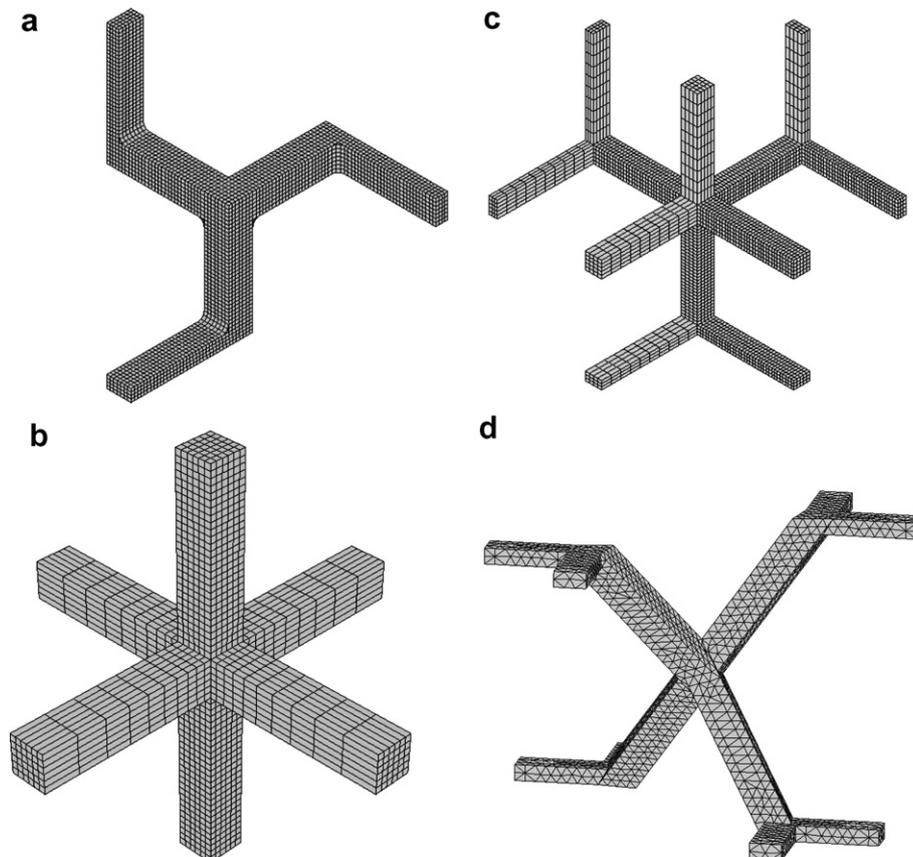
Fig. 2. Unit cell used for FEM calculations (constant relative density of 2.6%): (a) B model; (b) C model; (c) combination BC model; and (d) S model. The compressive stress is applied vertically.

buckle in an S shape and this model is thus referred to as the S model.

The four models were studied with the ABAQUS software package (version 6.51). Quadratic, cubic elements (C3D20) were used for all the models except the S model, where quadratic, tetrahedral elements (C3D10) were used. The effect of the number of elements was examined and found to be small. In the worst case of the S model, a factor of 6 increases in the number of elements resulted in less than a 4% relative change in strain rate at 5% strain.

Mirror planes were used to constrain the FEM nodes intersecting the six sides of the cubic models, which thus remained flat and parallel in the three orthogonal space directions. These constraints simulate an infinitely repeating structure and thus capture interactions between neighboring cells. A single FEM node at the lower side of the cube was fully constrained to prevent translation of the whole model owing to numerical round-off errors. Symmetry and boundary conditions allowed the use of a constant force applied to each FEM node intersecting the upper face of the structures for all but the BC model. For the BC model, a rigid plate was used to apply a uniaxial compressive stress on the upper face, allowing load transfer among vertical struts in the cell.

The models first deformed elastically and then underwent plastic deformation according to the creep power law given by Eq. (2) without primary creep. Creep parameters are shown in Table 1 for two materials: (i) Al-6101 (Al–0.6 wt.% Mg–0.5 wt.% Si) in the T6 condition [5], referred to as Al in the following and (ii) Ni–8 wt.% Al heat-treated to form γ' precipitates [13], referred to as Ni–8Al in the following. The average foam engineering strain was determined by dividing the displacement of the upper model face by the height of the cubic model.

Three parametric studies were performed for each of the four models. First, the foam relative density was varied from 2.6% to 14% by altering the strut cross-section while maintaining constant strut length. The compressive stress and temperature were fixed at 0.42 MPa and 275 °C and the materials parameters were those for Al-6101, allowing comparison with experimental creep results on Al-foams by Andrews et al. [5]. Second, the foam compressive stress was varied from 0.08 to 0.8 MPa, using a constant relative density of 2.6% and a temperature of 825 °C, with creep parameters for Ni–8Al to compare with experimental Ni–

8Al foam results by Choe and Dunand [13]. Third, the temperature was varied from 625 to 875 °C for the Ni–8Al foam with density of 2.6% at a constant compressive stress of 0.23 MPa and results were compared with experimental Ni–8Al foam creep data by the same authors [13].

3. Results

3.1. Foam creep curves and stress distribution

Creep curves, showing strain rate vs. strain (both tensile and compressive), are shown in Fig. 3 for each of the four models, using Ni–8Al creep parameters for a foam with a 2.6% relative density subjected to an uniaxial stress of 0.4 MPa at 825 °C. For the B and S models, the strain rate initially decreases rapidly by about one order of magnitude until an average foam strain of $\sim 0.5\%$ is achieved. This primary-like regime is followed by a secondary-like regime where the strain rate is nearly constant at $\sim 3 \times 10^{-2}\ \mathrm{s}^{-1}$ for compression and slowly decreases to $1 \times 10^{-2}\ \mathrm{s}^{-1}$ in tension, over the 0.5–8% strain range. By contrast, the C and BC models show no significant primary regime. The C model displays a nearly constant strain rate of $\sim 1.5 \times 10^{-6}\ \mathrm{s}^{-1}$ over the whole range of foam strain (0–8%) in compression, decreasing again by a factor of two over this range in tension. The BC model exhibits the largest difference between compressive and tensile deformation. For the latter mode, a nearly constant strain rate of $\sim 1 \times 10^{-5}\ \mathrm{s}^{-1}$ is maintained up to 8% strain, while for the former, a rapid increase by two orders of magnitude occurs over the 2–8% strain range. In the following, only compressive stresses were used, since they represent the most important mode of deformation for foams.

The effect of hollow struts was examined for the B model with relative density of 2.6%, using square beams with a

Table 1
Creep properties used for FEM calculations

Material	Creep constant A (MPa^{-n} s^{-1})	Stress exponent n (–)	Activation energy Q (kJ mol^{-1})	Remarks	Ref.
Ni–8Al	4.21×10^{-5}	5.8	230	Ni–8 wt.%Al after γ' precipitation aging	[13]
Al	1.95×10^{3}	4.0	173	Al-6101 in T6 condition	[5]
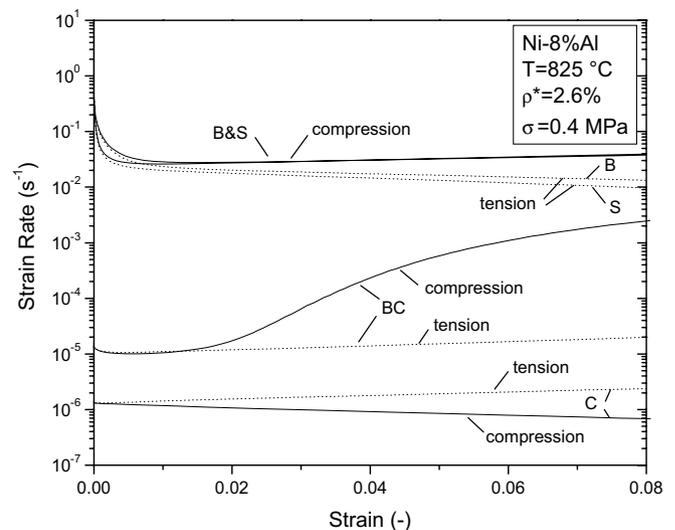
Fig. 3. Calculated creep curves for all four models using Al creep properties (stress: $\sigma = 0.4$ MPa; temperature: $T = 825$ °C; relative density: $\rho = 2.6\%$).
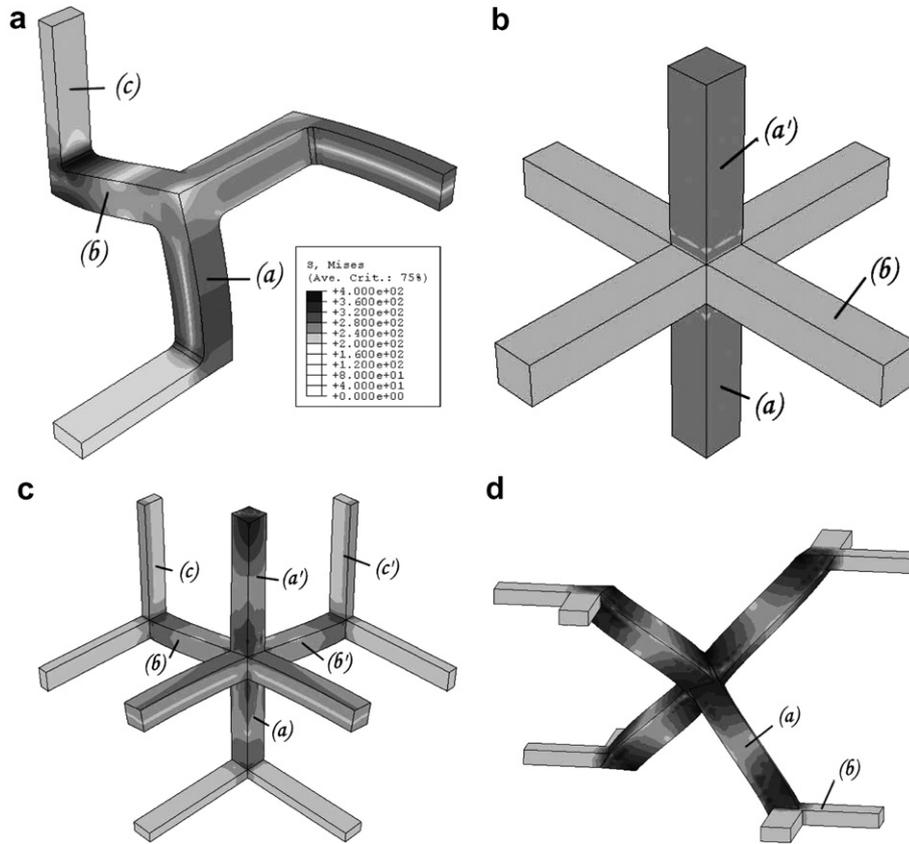
Fig. 4. Unit cell after creep deformation to an average compressive strain of 5% for the Al foams ($\sigma = 0.42$ MPa, $T = 275$ °C, and $\rho = 2.6\%$): (a) B model; (b) C model; (c) combination BC model; and (d) S model. Displacements are magnified by a factor of two and the von Mises stress contours are plotted using the same 0–400 MPa scale.

ratio of wall thickness to strut width of 0.3 for an Al foam (with 0.42 MPa stress at 275 °C). The creep curve for hollow strut model was offset over the 0–5% strain range by a factor ~2.5 on the strain rate axis with respect to the curve for non-hollow struts. This decrease in strain rate, which is qualitatively expected given the higher bending stiffness of hollow struts, is quantitatively small enough to be ignored in the present study which focuses on non-hollow struts.

Fig. 4a–d shows the four models after creep deformation at 275 °C to an average strain of 5% for the Al foam with 2.6% relative density subjected to a 0.42 MPa compressive stress. Displacements are magnified by a factor of two to help visibility and the von Mises stress contours are plotted using the same 0–400 MPa scale to allow direct comparison between the models. It is apparent that stress concentrations are minimal for the C and BC models and much more pronounced, especially near the nodes, in the B and S models. Vertical struts, initially in uniaxial compression, tend to deflect laterally (except for the C model) and non-vertical struts show pronounced bending deflections.

3.2. Foam average strain rate

Fig. 5 shows the average secondary compressive foam creep rates (determined at 1% average strain for all models and also at 5% for the BC model) as a function of applied

stress for the Ni–8Al foams at constant temperature and relative density ($T = 825$ °C, $\rho = 2.6\%$). The strain rates predicted by the two simplest FEM models (B and C mod-
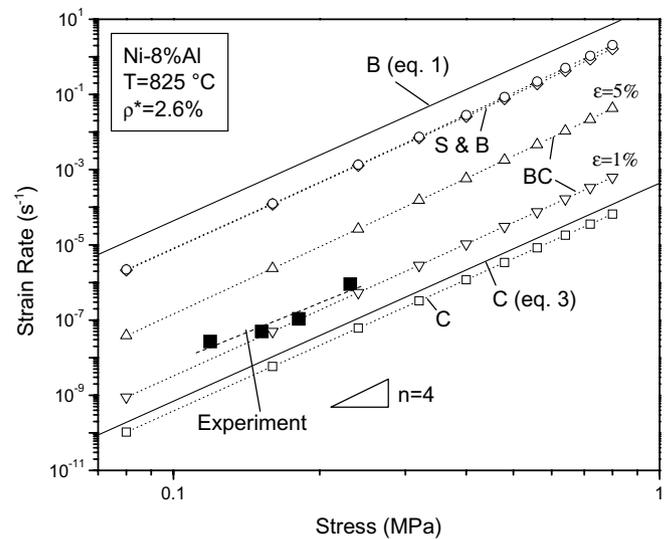
Fig. 5. Compressive stress dependence of average foam compressive creep rates determined by FEM for all models (hollow symbols) and calculated using Eqs. (1) and (3) for the B and C models (lines), using Ni–8Al creep properties ($T = 825$ °C, $\rho = 2.6\%$). Experimental data for Ni–8Al foams [13] are also plotted as full symbols.

els) are separated by over four orders of magnitude. The slopes of the curves in Fig. 5 correspond to the foam stress exponents, which are nearly identical to those of the Ni–8Al base material, as predicted by the respective analytical solutions (Eqs. (1) and (3)). However, the strain rates predicted by FEM are lower than those predicted by the analytical models, by a factor 5 for the B and two for the C models. Comparing numerical models, the S model gives results that are very close to the numerical B model, while the BC model predicts strain rates intermediate between the two extremes given by the B and C models. Only the BC model shows significant differences between strain rates calculated at 1% and 5% foam strain, as expected from the compressive creep curves shown in Fig. 3.

Fig. 6 shows the temperature dependence of the foam creep rate for Ni–8Al foams at constant stress and relative density ($\sigma = 0.23$ MPa, $\rho = 2.6\%$). As in Fig. 5, the B and S numerical predictions for strain rates are much higher than for the C model (by about four orders of magnitude), while the BC model lies between these extremes. Also as in Fig. 5, the analytical B and C solutions provide higher strain rates than the numerical models (by factors 5 and 2, respectively), but with similar slopes, corresponding to the activation energy of the Ni–8Al base material.

For both stress- and temperature-dependences (Figs. 5 and 6), the experimental data for Ni-alloy foams (with 8–9%Al and relative density 2.5–2.6% [13]) are close to predictions from the BC model at 1% strain and tolerably close (within one order of magnitude) to the numerical and analytical C models. By contrast, the B and S models predict strain rates that are much higher (by three orders of magnitude) than measured experimentally.
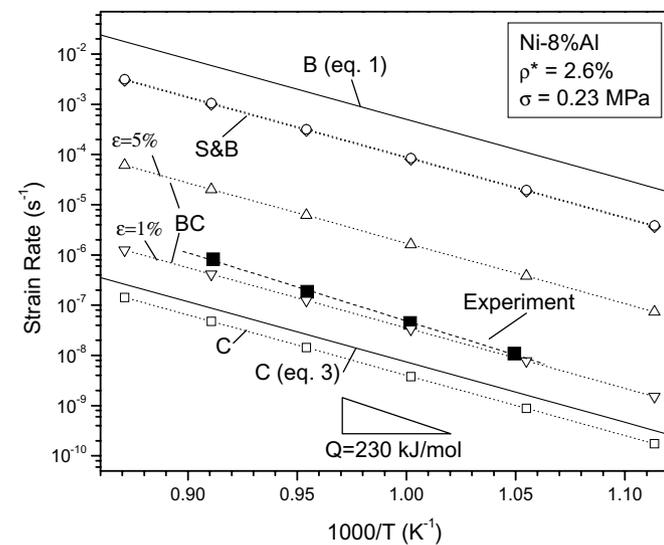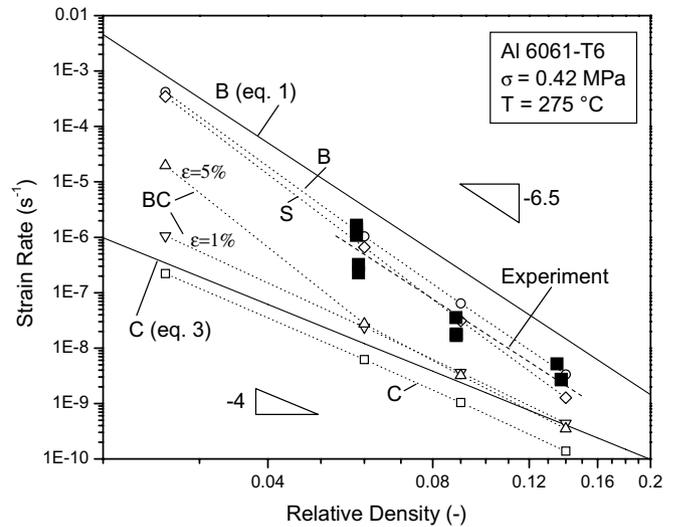
Fig. 7. Density dependence of average foam compressive creep rates determined by FEM for all models (hollow symbols) and calculated using Eqs. (1) and (3) for the B and C models (lines), using Al creep properties ($\sigma = 0.42$ MPa, $T = 275$ °C). Experimental data for Al foams [5] are also plotted as full symbols.

Finally, the creep rate is plotted in Fig. 7 as a function of relative density for Al foams at constant stress and temperature ($\sigma = 0.42$ MPa, $T = 275$ °C). Here again, numerical B and S models provide strain rates that are very close to each other and below the B analytical model (Eq. (1)), the numerical C model predicts much lower strain rates that are close to the analytical C model (Eq. (3)) and the BC model provides intermediate strain rates. The experimental creep rate data by Andrews et al. [5] for Al foams with relative densities of 6%, 9% and 14%, are close to predictions from the numerical B and S models and are within one order of magnitude of the BC model predictions.

4. Discussion

4.1. Foam strain and stress distribution

The geometry of the models can be discussed by comparing the unit cells in Fig. 2. While these cells display the same relative density, their architecture varies and these differences can be quantified by defining various geometrical parameters. A first parameter is the volume fraction of struts non-parallel to the applied stress, calculated by sharing equally the node material between its respective struts. This volume fraction is 0.67 for the B, C and BC models and 0.42 for the S model. The relevance of this parameter is that non-parallel struts are expected to deform primarily by bending, contributing much less to the cell creep resistance than parallel struts which deform primarily by compression. A second geometrical parameter is the average number of struts converging into nodes: the higher this number, the more constrained the struts are, thus increasing their stability towards lateral deflection. This number is 3, 4, 4.5 and 6 for the B, S, BC and C models, respec-

Fig. 6. Temperature dependence of average foam compressive creep rates as determined by FEM for all models (hollow symbols) and calculated using Eqs. (1) and (3) for the B and C models (lines), using Ni–8Al creep properties ($\sigma = 0.23$ MPa, $\rho = 2.6\%$). Experimental data for Ni–8Al foams [13] are also plotted as full symbols.

tively. This same series also describes creep resistances (Figs. 5–7), as expected. A third parameter is the average strut aspect ratio, which affects the average bending moment of non-parallel struts. This average aspect ratio increases from 3.5, 5.2, 5.4 to 9.4 for the B, S, BC and C models, respectively (calculated for a 2.6% relative density). It is thus apparent that the four model architectures differ readily from each other and that these differences affect the details of creep deformation, as discussed below by examining unit cells having accumulated an overall strain of 5% (Fig. 4a–d).

For the B model in compression (Fig. 4a), plastic hinging is visible in the form of stress concentrations near both nodes of the horizontal strut (b) connecting the two vertical struts (a) and (c). The central vertical strut (a) deflects from its initially vertical position (where it is originally subjected to pure uniaxial compression) first elastically and subsequently by creep. This lateral deflection reduces the average bending moment on strut (b), leading to a geometric hardening explaining the primary creep region (Fig. 3) where the deformation rate rapidly decreases in the 0–0.5% foam strain range. This also provides an explanation for the lower overall minimum strain rate determined by FEM compared to Eq. (1), as seen in Figs. 5–7. In fact, the initial FEM strain rate near 0% foam strain (Fig. 3) is close to the analytical value provided by Eq. (1), which does not assume lateral deflection of strut (a). The situation is similar in tension, for which an analogous primary behavior is observed in Fig. 3. The slight increase in compressive strain rate in the secondary regime (Fig. 3) is probably due to stress concentrations in the two plastic hinges of strut (b). The severity of the stress concentration is reduced in tension compared to compression (owing to the asymmetry in the (a–c) strut assembly), explaining the lower secondary strain rates in tension.

In the C model in compression (Fig. 4b), by contrast, there is no lateral deflection of the two vertical struts (a) and (a′) which remain in pure uniaxial compression throughout foam deformation. Their cross-sections vary as strain accrues and this decreases the local stress in compression (respectively, increases it in tension), explaining the slight decreases (respectively, increases) in strain rate with increasing strain visible in Fig. 3. For a Ni–8Al foam strain of 8%, this effect reduces (respectively, amplifies) the strut strain rate by a factor $1.08^n = 1.6$. Also relevant is the reduced stress levels in the node connecting the two vertical struts (a) and (a′), caused by the confining effect of the four horizontal struts (b). Both effects are relatively minor, leading to a discrepancy from the analytical model (Eq. (3)) of about a factor two (Figs. 5–7). However, the latter effect becomes more important as the volume fraction (and thus the node size) increases, explaining the slight divergence between the analytical and FEM lines in Fig. 7.

The combination BC model (Fig. 4c) exhibits a complex temporal evolution of stress in compression. First, load is carried both by the central vertical struts (a–a′) acting as a continuous column (as in the C model) and

by the lateral vertical struts (c) and (c′) which bend the connecting horizontal struts (b) and (b′), as in the B model. This lateral deflection of the central struts (a–a′) is however much less pronounced than in the B model and so the primary stage in the BC model is also much reduced compared to the B model. Unique to the BC model is the evolution of the compressive stress carried by the vertical struts, with load being transferred from the central vertical struts (a–a′) to the lateral vertical struts (c) and (c′) as the former deflects laterally. The resulting increase in bending force on the horizontal struts (b) and (b′) explains the steadily increasing strain rate, observed in Fig. 3. This effect is much less pronounced for higher density BC models (Fig. 6), for which the central vertical struts resist lateral deflection better and become stronger owing to their increased cross section. In tension, however, the central vertical struts (a–a′) do not deflect laterally, so that the strain rate remains nearly constant with increasing strain, as seen in Fig. 3.

Finally, the S model in compression (Fig. 4d) is characterized by complex bending moments leading to an S-shaped deflection of the four struts (a) oriented at a 45° angle with respect to the applied stress. As for the B-model, deflection of these struts reduces their average moment and thus leads to slower creep deformation, explaining the primary creep stage. Also as for the B model, stresses are concentrated near the nodes, leading to plastic hinging conditions. The horizontal struts (b) are nearly non-load bearing (as for some of the horizontal struts in the C and BC models), but provide resistance against lateral deflections of the nodes. The situation is symmetric in tension, leading to the same primary behavior. In the secondary regime, the slight increase (for compression) and decrease (for tension) in strain rate are due to increase (respectively, decrease) in average bending moment for the (b) struts, as they deflect from their initial 45° angle with respect to the applied stress.

4.2. Comparison between B and S models

The B and S models exhibit almost exactly same strain rate evolution (Fig. 3) and dependence on stress, temperature and volume fraction (Figs. 5–7). This was initially surprising as it was assumed that the S model would result in strain rates intermediate between those of the B and C models, since the load-bearing struts (a) display a 45° angle intermediate between vertical (as in the C model) and horizontal (as in the B model). Also, the strut aspect ratios and node connectivity are quite different, as discussed previously.

However, when the B and S models are compared in terms of beam theory, it becomes clear that, despite the different architectures, the predicted deflection rates of the central bending struts (strut (b) for the B model and strut (a) for the S model) are nearly equal. This is demonstrated by a simplified 2D analysis: for the B model, this analysis leads to Eq. (1), which considers that the horizontal strut

(b) in Fig. 4a deflects by bending in the direction of the applied stress, while the vertical struts (a) and (c) remain rigid and aligned with the applied stress. The vertical deflection rate $\dot{\delta}$ of the horizontal strut (b) is given by Ref. [1]:

$$\dot{\delta}_B \propto \frac{l^{n+2} F_B^n}{t^{3n+1}} \qquad (4)$$

where l and t are the strut length and thickness and F_B is the force component acting in the vertical direction on strut (b) (Fig. 4a). The strut length l is given by $l' - t$, where l' is the distance between the centers of the two nodes at the end of the strut.

For the S model, the deflection in the vertical direction due to bending of strut (a) in Fig. 4d can be written as

$$\dot{\delta}_S \propto \frac{l^{n+2} (F_S \cos(\theta))^n}{t^{3n+1}} \cos(90° - \theta) \qquad (5)$$

where F_S is the force acting in the vertical direction on strut (a) and $\theta = 45°$ is the angle between this force and the strut longitudinal axis. The ratio for the strut deformation rate of both models, with $F_S = 2F_B$, is then:

$$\frac{\dot{\delta}_B}{\dot{\delta}_S} = 2^{(1-n)/2} \left(\frac{l_B}{l_S} \right)^{n+2} \left(\frac{t_B}{t_S} \right)^{-(3n+1)} \qquad (6)$$

This ratio is independent of stress and temperature and depends on volume fraction through the ratios (l_B/l_S) and (t_B/t_S). These ratios vary in the range 0.46–0.40 and 0.69–0.65, respectively, for the present range of relative densities ($\rho = 2.6$–14%, corresponding to ratios of strut length/thickness varying in the range 3.5–0.9 and 5.2–1.5 for the B and S models, respectively). Evaluating Eq. (6) over this range of relative densities for a physically relevant range of stress exponents ($n = 1$–6), it is found that the ratio of strut deflections in the vertical direction is remarkably constant and close to unity, remaining within the narrow range 0.23–0.50.

This simplified 2D analysis thus predicts that the B model should exhibit a strain rate lower by factors 2–4 than the S model. This difference is much less than the many orders of magnitude in strain rate difference between the B and C models. As shown in Fig. 4a and d for the 3D FEM analysis, deformation also occurs in the vertical struts of the B model and it takes place by a more complex mode than simple bending of the strut (a) in the S model. Also, the beam cross-section for strut (a) in the S model is tilted with respect to the applied stress. All these effects are relatively small compared to the bending of the struts discussed above, so the ratio in Eq. (6), which is close to unity, is a good approximation for the ratio of foam strain rates for the two models.

4.3. Foam average strain rate

For all models, there was a critical strain of 5–10% at which unstable creep buckling took place, leading to very rapid increases in compressive creep rates. In real foam specimens with stochastic cell architectures, such instabilities are localized in small volumes of the sample; they either are compensated by load transfer to stronger regions, or propagate to form a crush band spanning the whole sample area but with a height much less than that of the sample. In the present FEM model, such instabilities affect the whole sample owing to the periodicity of the boundary conditions and are thus not representative of the true behavior of a stochastic foam.

Comparing the two models for which analytical expressions exist, (Eq. (1) for B and Eq. (3) for C), it is apparent that the compressive stress-, temperature- and (to a lesser extent) density-sensitivity of the strain rate is nearly the same for the numerical and analytical models and correspond to the bulk stress exponent n, bulk activation energy Q and density exponents ($-(3n + 1)/2$ for Eq. (1) or $-n$ for Eq. (3)), respectively. However, the numerical discrepancy between calculated and analytical strain rates is much higher for the B model, as discussed earlier. The S model displays tetrakaidecahedral geometry, which is more complex and thus often considered to be more realistic than the simple bending geometry used for the B model. Nevertheless, the S model provides numerical results very close to those of the B model, as discussed above. Finally, the BC model provides the same stress- and temperature-sensitivities as both B and C models, but a density exponent (for relative densities higher than 6%) that is closer to the value of $-n$ for the C model than to the value of $-(3n + 1)/2$ for the B model. In the logarithmic plots of Figs. 5–7, the strain rate for the BC model is closer to the C model than to the B and S models (except at the lowest relative density of 2.6% for a strain of 5%).

The relative density study (Fig. 7) shows that the numerical models are more sensitive to density than expected by theory: the slopes are -4.4 and -4.6 for the C and BC models (compared to -4 from Eq. (3)) and -7.0 and -7.5 for the B and S models (compared to -6.5 from Eq. (1)). The following explanations can be advanced for this effect. As relative density decreases, the aspect ratio of the struts increases thus increasing the tendency for the vertical strut (a) to deflect laterally in the B model and decreasing the relative size of the node volume bearing less stress than the vertical struts (a) and (a') in the C model.

The large spread in strain rates between the two extreme cases given by the B and C models shows that architecture has a strong influence on the foam creep resistance. This is apparent in the comparison with experimental data in Figs. 5–7: the Ni–8Al data are close to the BC model predictions at 1% strain, while the Al foam data are much closer to the B or S models. Agreement with particular models may be fortuitous given that these models are highly anisotropic owing to the use of a single unit cell repeated through boundary conditions in a cubic lattice: for instance, faster creep rates are expected for the BC model if the loads are not parallel to the vertical columns. However, it is interest-

ing that experimental creep rates of the Ni–8Al foams are closer (on a logarithmic scale) to the lower extreme case (model C), while those for the Al foams are closer to the upper extreme case (model B). These differences probably reflect variations in geometries and architectures caused by the different modes of fabrication for these two foams, leading to a higher proportion of compressive strut deformation for the Ni–8Al foams and a higher proportion of strut bending for the Al foams. It is thus clearly advantageous to achieve foams with a high proportion of continuous struts oriented in the direction of the load, similar to oriented fibers in a composite.

5. Conclusions

Creep of cellular materials was modeled by the finite element method for four 3D unit cells: (i) the B model, where bending of struts perpendicular to the applied stress is dominant; (ii) the C model, where compression of struts parallel to the applied stress is dominant; (iii) the BC model, combining perpendicular struts deforming by bending (as for the B model) and parallel struts deforming by compression (as for the C model); (iv) the S model, with a tetrakaidecahedral geometry where struts forming a 45° angle with the applied stress deform into a S shape owing to complex bending moments. The following conclusions can be drawn from parametric studies on these four models, where compressive creep curves were calculated for average foam strains of 0–5%, while systematically varying stress, temperature and foam density using creep constants for Al and Ni alloy foams:

- For the B model, an initially high creep rate decays over the strain range 0–0.5% caused by bending of both vertical and horizontal struts. This primary regime is followed by a secondary regime where the creep rate is roughly constant.
- The S model gives rates very close to those of the B model, caused by bending struts deforming at similar rates in both models, despite exhibiting different aspect ratios and angles with respect to the applied stress.
- The C model is characterized by secondary regime without primary regime. Deformation is mainly by compression of the parallel struts.
- The BC model also exhibits a secondary regime without primary regime up to 1% strain, beyond which a ternary regime appears at low foam density, where the strain rate increases steadily as a result of load transfer between struts.
- The highest secondary creep rates are predicted by the B and S models, but are slower by about a factor 10 compared to a simplified 2D analytical solution for the B model (Eq. (1)). The lowest secondary creep rates are predicted by the C model and are within a factor of two of the simplified 2D analytical prediction (Eq. (3)). Both B and C numerical models exhibit the same stress, temperature and (to a lesser extent) density

dependence as their respective analytical 2D solutions (Eqs. (1) and (3)). The BC model predicts secondary creep rates that are intermediate between those of the B and C model.
- Published experimental creep data on Ni–8Al foams, where stress or temperature were varied, are close to the lower extreme given by the C model, while published experimental data on Al foams, where density was varied, are close to the upper range given by the B model, illustrating the importance of foam architecture upon their creep resistance.

Acknowledgements

References

[1] Ashby MF, Evans A, Fleck NA, Gibson LJ, Hutchinson JW, Wadley HNG. Metal foams: a design guide. Oxford: Butterworth-Heinemann; 2000.

[2] Andrews EW. Open-cell foams with hollow struts: mechanical property enhancements. Mater Lett 2006;60:618.

[3] Andrews EW, Gibson LJ. The role of cellular structure in creep of two-dimensional cellular solids. Mater Sci Eng A 2001;303:120.

[4] Andrews EW, Huang JS, Gibson LJ. Creep behavior of a closed-cell aluminium foam. Acta Mater 1999;47:2927.

[5] Andrews EW, Gibson LJ, Ashby MF. Overview no. 132: the creep of cellular solids. Acta Mater 1999;47:2853.

[6] Hodge AM, Dunand DC. Measurement and modeling of creep in open-cell NiAl foams. Metall Mater Trans A 2003;34A:2353.

[7] Choe H, Dunand DC. Mechanical properties of oxidation-resistant Ni–Cr foams. Mater Sci Eng A 2004;384:184.

[8] Zurob HS, Brechet Y. Effect of structure on the creep of open-cell nickel foams. J Mater Sci 2005;40:5893.

[9] Zhang P, Haag M, Kraft O, Wanner A, Arzt E. Microstructural changes in the cell walls of a closed-cell aluminium foam during creep. Philos Mag A 2002;82:2895.

[10] Hakamada M, Nomura T, Yamada Y, Chino Y, Chen YQ, Kusuda H, et al. Compressive deformation behavior at elevated temperatures in a closed-cell aluminium foam. Mater Trans 2005;46:1677.

[11] Haag M, Wanner A, Clemens H, Zhang P, Kraft O, Arzt E. Creep of aluminium-based closed-cell foams. Metall Mater Trans A 2003;34A:2809.

[12] Hakamada M, Nomura T, Yamada Y, Chino Y, Hosokawa H, Nakajima T, et al. Compressive properties at elevated temperatures of porous aluminium processed by the spacer method. J Mater Res 2005;20:3385.

[13] Choe H, Dunand DC. Synthesis, structure and mechanical properties of Ni–Al and Ni–Cr–Al superalloy foams. Acta Mater 2004;52:1283.

[14] Gibson L, Ashby M. Cellular solids: structure and properties. 2nd ed. Cambridge: Cambridge University Press; 1997.

[15] Kesler O, Crews LK, Gibson LJ. Creep of sandwich beams with metallic foam cores. Mater Sci Eng A 2003;341:264.

[16] Lin JY, Huang JS. Creep-buckling of hexagonal honeycombs with plateau borders. Compos Sci Technol 2006;66:51.

[17] Cocks ACF, Ashby MF. Creep-buckling of cellular solids. Acta Mater 2000;48:3395.

[18] Andrews E, Sanders W, Gibson LJ. Compressive and tensile behaviour of aluminium foams. Mater Sci Eng A 1999;270:113.

[19] Zhu HX, Hobdell JR, Windle AH. Effects of cell irregularity on the elastic properties of open-cell foams. Acta Mater 2000;48: 4893.

[20] Huang JS, Gibson LJ. Creep of open-cell Voronoi foams. Mater Sci Eng A 2003;339:220.

[21] Zhu HX, Mills NJ. Modelling the creep of open-cell polymer foams. J Mech Phys Solids 1999;47:1437.

[22] Zhu HX, Knott JF, Mills NJ. Analysis of the elastic properties of open-cell foams with tetrakaidecahedral cells. J Mech Phys Solids 1997;45:319.